NASA CONTRACTOR REPORT

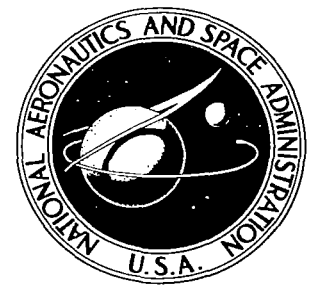

NASA CR-318

NASA CR-385

A COMPARISON OF THEORETICAL AND EXPERIMENTAL PRESSURES AND FORCES ACTING ON A RING BAFFLE UNDER SLOSHING CONDITIONS

by Luis R. Garza

Prepared under Contract No. NAS 8-1555 *by*
SOUTHWEST RESEARCH INSTITUTE
San Antonio, Texas
for George C. Marshall Space Flight Center

NATIONAL AERONAUTICS AND SPACE ADMINISTRATION • WASHINGTON, D. C. • MARCH 1966

NASA CR-385

A COMPARISON OF THEORETICAL AND EXPERIMENTAL PRESSURES AND FORCES ACTING ON A RING BAFFLE UNDER SLOSHING CONDITIONS

By Luis R. Garza

Prepared under Contract No. NAS 8-1555 by
SOUTHWEST RESEARCH INSTITUTE
San Antonio, Texas

for George C. Marshall Space Flight Center

NATIONAL AERONAUTICS AND SPACE ADMINISTRATION

For sale by the Clearinghouse for Federal Scientific and Technical Information
Springfield, Virginia 22151 – Price $2.00

ABSTRACT

A comparison is presented of non-dimensionalized theoretical and experimental pressures and forces acting on a flat ring baffle under sloshing conditions. Comparisons are made for various baffle depths and for three values of tank excitation amplitudes. Force measurements for various perforated baffles are also presented.

LIST OF SYMBOLS

a	Longitudinal acceleration of tank
d	Cylindrical tank diameter
d_s	Distance from top of baffle to liquid surface
h	Liquid depth to bottom of tank
R	Cylindrical tank radius
W	Baffle width
X_o	Tank excitation amplitude in translation
ω_n	Liquid natural circular frequency
ζ	Liquid slosh height
P	Pressure
F	Force

INTRODUCTION

Ring baffles as liquid damping devices in cylindrical tanks and their effect on resonant frequencies were investigated in Ref. 1. The present report is a continuation of this work, with emphasis on the ring pressure distribution and total baffle loading force under sloshing conditions.

The ring baffles considered in this report are similar to those in Ref. 1, and the equipment and procedures are similar to those in Ref. 2. The pressure and baffle forces were recorded for three excitation amplitudes at frequencies corresponding to the maximum baffle loading.

A comparison is presented of the experimental pressure and force measurements with theoretical values computed from Refs. 3 and 4. Experimentally determined liquid slosh heights and resonant frequencies were employed in the theoretical computations.

TANK CONFIGURATION

An 11.5" diameter plastic tank was used for all the pressure and baffle load measurement tests rather than the 1.2 ft diameter steel tank used in Ref. 1. The steel tank was found to have various irregular and out-of-round sections which would have been detrimental to the baffle force system.

The ring baffle for these tests was split in half, one attached rigidly to the tank wall surface and the other half supported by three force measuring dynamometers, as shown in Figure 1. Also shown in Figure 1 are five pressure sensing beam elements which were soldered at cut-out sections around a 90^{o} baffle section. During the tests, the vertical uprights attaching the baffle half to the dynamometers were oriented in line with the tank excitation amplitude offering little or no distortion to the liquid flow pattern, as shown in Figure 2. A nominal clearance of approximately 0.01" to 0.02" was maintained between the instrumented baffle and the tank wall by the round aluminum dynamometer support fixture. The aluminum fixture, with a nominal diameter approximately 0.020" greater than the baffle diameter, was machined for a press fit into the plastic tank. The assembly was simplified by the use of a heat gun which expanded the plastic tank and allowed easy positioning of the aluminum fixture. Upon completion of pressure distribution tests, force

measurements on various perforated baffles were conducted by fixing the baffle similarly to the instrumented solid baffles.

The baffle heights were simply altered by addition or draining of the test fluid. All tests were conducted for $h/d > 1$ and the following dimensionless tank excitation amplitudes: $X_o/d = 0.00417$, 0.0083 and 0.0107. The slosh heights necessary for the theoretical baffle pressure and baffle force values were recorded visually and with capacitive probes. The visual measurements proved to be more efficient in that the gross motion of the liquid height was averaged more easily.

PRESSURES ON RING BAFFLES

Tests were conducted in a tank in forced excitation, driven horizontally in a steady harmonic motion at the first liquid resonant frequency or at a slightly higher frequency corresponding to a maximum baffle loading. Pressure data were recorded for baffle depths (d_s/R) ranging from $d_s/R = 0$ to $d_s/R = 0.375$, in increments of $d_s/R = 0.025$. These tests were conducted for three tank excitation amplitudes (X_o/d) ranging from $X_o/d = 0.00417$ to $X_o/d = 0.0107$.

The data reduction for baffle depths greater than $d_s/R = 0.075$ was by a harmonic analysis method which resulted in peak to peak pressure amplitudes. For a baffle depth less than $d_s/R = 0.075$, the zero line was easily detected, and the peak positive pressure was measured and then doubled for consistent peak to peak pressure presentation.

Plots of the test data indicated that the peak pressure (in the plane of excitation) varied almost directly with the tank excitation amplitude (X_o/d). Because of the linear excitation amplitude relationship with the pressure measurements, it was decided to present the data results as a root-mean-square value for the three test excitation amplitudes.

Experimental data for all excitation amplitudes are presented in tabular form in Appendix A.

In conducting these tests, a large number of them were re-run to determine whether the baffle pressure followed the predicted cosine distribution, as indicated in Ref. 3. After many tests and a careful study of the liquid motions, it was determined that the experimental pressures could not follow a cosine distribution because of the liquid slosh pattern. The liquid slosh which produces maximum baffle loading is not a pure anti-symmetrical slosh mode; rather it is a combination of an anti-symmetrical and symmetrical slosh mode, as can perhaps be seen in Figure 3 (note the anti-symmetrical and the symmetrical slosh with the concave shape away from the liquid center). Reference 5 also mentions this type of liquid sloshing.

The experimental pressure measurements agree very closely with the theoretical values (Ref. 3) for the baffle section normal to the excitation amplitude. Figures 4 and 5 present the comparison of the non-dimensional, experimental and theoretical pressures values $(P/\ aX_o)$ for two radial locations at the baffle section normal to the excitation amplitude $\theta = 0$. Figure 6 presents the pressure comparison for $\theta = 30^o$. Although not as close as those presented in Figure 5, the theoretical pressures are still reasonably close and could be considered as valid pressures in any baffle design. Figure 7 presents the comparison for $\theta = 60^o$. The major difference between the theoretical and experimental pressures is a direct result of the symmetrical component of the

sloshing mode. A harmonic analysis of the data indicated that, for this baffle section, approximately 24% of the pressure amplitude resulted from the symmetrical slosh component. The pressure recorded at $\theta = 85^{\circ}$ was very erratic, and no attempt was made to reduce the data. Visual observation of the data indicates that the apparent pressure component for $\theta = 85^{\circ}$ was primarily due to the symmetrical sloshing mode.

No pressure data were recorded for perforated ring baffles. Tests on perforated ring baffles were limited to the total loading force measurements, and the results are presented in the following section.

Appendix B presents the theoretical formulation employed, from Ref. 3.

BAFFLE LOADING FORCE MEASUREMENTS

Baffle force data were recorded for solid (non-perforated) baffles and various perforated baffles. The data were recorded as a peak-peak force measurement on half of the baffle normal to the direction of translational excitation. The other half of the baffle was rigidly attached to the tank wall surface. As in the case of the pressure data, the force measurements were found to be quite linear with the excitation amplitude (X_o/d).

The force measurements for all the baffles considered are presented in terms of dimensionless force ($F/\rho ad^3(X_o/d)$) versus the baffle submergence depth (d_s/R). The force values are the root mean square values obtained for three values of tank translation excitation amplitude.

Figure 8 shows a comparison of the experimental force measurements and two theoretical force values computed from Refs. 3 and 4. Experimentally determined liquid slosh heights and resonant frequencies were used in the theoretical computations. It can be seen from Figure 8 that the experimental values are in the range bounded by the two theoretical computations.

A comparison of the experimental force values and those computed from Ref. 3 again illustrate that the pressure for the baffle section, where $\theta = 60^o$, is significant and constitutes the difference

between the theoretical and experimental force data. The theoretical values computed from Ref. 4 are greater than the experimental values and would appear to be safe for design purposes. The significant criteria for design purposes is the maximum baffle loading. From Figure 8, it can be seen that the maximum baffle loading occurs when the baffle is located at the liquid free surface, $d_s/R = 0$. For this depth ($d_s/R = 0$), the theoretical values of Ref. 3 appear to be much closer than are those computed from Ref. 4.

Baffle loading forces were also recorded for various perforated baffles. Figure 9 presents a comparison of the baffle forces for a solid ring baffle with various perforated baffles. For this comparison, the perforation hole size is kept constant at $d_h = .079"$, and various percentages of perforated open areas are considered. It can be seen from this figure that the baffle loading is decreased considerably for the 8% and 16% open areas, but no significant additional decrease in force is noted for the 23% and 30% over the 16% open baffle.

Figure 10 presents a comparison of the baffle forces for a solid ring baffle with various 30% open baffles having different hole size openings. It may be noted that the baffle force increases as the perforation hole size is decreased. Additional perforated baffle tests must be conducted on other tank diameters to establish a relationship between baffle perforation hole size and tank diameter.

CONCLUSIONS

The comparisons of the theoretical and experimental pressures are based on the liquid slosh height, obtained from visual measurements. Capacitive probe-type slosh height measurements were also recorded, but these were discarded because the measurements were not representative of the complex mode liquid slosh encountered with baffles near the liquid free surface.

The comparisons generally appear to be in very good agreement. The pressure distributions also appear to be good for the baffle sector normal to the excitation amplitude ($\theta < 30^{o}$); for the baffle sector $\theta > 30^{o}$, the experimental pressures are considerably higher. The effect of the higher pressures at these angles can be noted in the comparison of the experimental force measurements and the forces computed from Ref. 3 using a cosine pressure distribution.

REFERENCES

1. Abramson, H. N., and Garza, L. R., "Some Measurements of the Effects of Ring Baffles in Cylindrical Tanks", Journal of Spacecraft and Rockets, 1 (5), Sept.-Oct. 1964, pp. 560-562.

2. Abramson, H. N. and Ransleben, G. E., Jr., "Simulation of Fuel Sloshing Characteristics in Missile Tanks by Use of Small Models", ARS Journal, 30, July 1960, pp. 603-612.

3. Liu, F. C., "Pressure on Baffle Rings Due to Fuel Sloshing in a Cylindrical Tank, NASA-MSFC Aero-Astrodynamics Internal Note 4-64, January 1964.

4. Handbook of Astronautical Engineering (edited by H. H. Koelle), Chapter 14: "Stability and Control", by G. L. Armstrong and K. Kachigan, Section 14.150, "Baffle Loads", pp. 14-25 to 14-27, McGraw-Hill, 1961.

5. Abramson, H. N., Chu, W. H., and Kana, D. D., "Some Studies of Nonlinear Lateral Sloshing in Rigid Containers", Final Report, Contract NASr-94(03), Southwest Research Institute, December 1964. NASA CR-375

X_o/d	d_s/R	P, psi (p-p) $\theta = 0^o$ y/W = .824	P, psi (p-p) $\theta = 0^o$ y/W = .32	P, psi (p-p) $\theta = 30^o$ y/W = .32	P, psi (p-p) $\theta = 60^o$ y/W = .32	F, lbs Semi-Baffle (p-p)
.0107	0	.0229	.0564	.0336	.0269	.395
↑	.025	.0195	.052	.053	.0215	.326
	.050	.0199	.0398	.0268	.0217	.304
	.075	.0154	.0362	.029	.0270	.330
	.100	.0117	.0334	.018	.0188	.335
	.125	.0110	.0350	.0233	.0220	.321
	.150	.0183	.0334	.0299	.0244	.362
	.175	.0158	.0375	.0485	.0287	.371
	.250	.0166	.0424	.0197	.0259	.414
↓	.300	.0151	.0455	.0237	.0287	.462
.0107	.375	.0210	.0512	.0223	.0285	.502
.0083	.000	---	---	---	---	.401
↑	.025	---	.0398	---	---	.287
	.050	.0161	.0338	.0166	.0205	.300
	.075	.0142	.0288	.0139	.0149	.273
	.100	.0088	.0291	.0148	.0226	.244
	.125	.0104	.0236	.0182	.0173	.233
↓	.175	.0106	.0288	.0241	.0194	.327
.0083	.250	.0147	.0332	.0189	.0217	.333
.00417	.250	.0096	.0176	.0162	.0145	.165
↑	0	---	---	---	---	.195
	.025	.0077	.025	.009	.0177	.173
	.050	.005	.0191	.0075	.016	.162
	.075	.0021	.0112	.009	.012	.116
↓	.100	.0033	.0138	.0132	.013	.104
.00417	.175	.008	.0121	.009	.0175	.146

PRESSURE AND FORCE DATA

APPENDIX B

According to Liu's general theory, the pressure on either side of the baffle is

$$\frac{1}{\rho} P(u,v) = \dot{U}\left\{R_e\left[AF(u,v)\right] - A_u\right\} - U^2\left[\tfrac{3}{2} - 2AR(u,v)f(u,v) + A^2R(u,v)/2K(u,v)\right]$$

for v = 0. u and v are the coordinates in the conformally mapped plane of the baffle. AF (u, v) is the mapping function, where A is a constant. K, R, and F are certain complex functions.

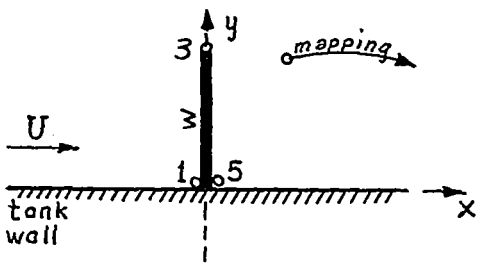

Physical Plane

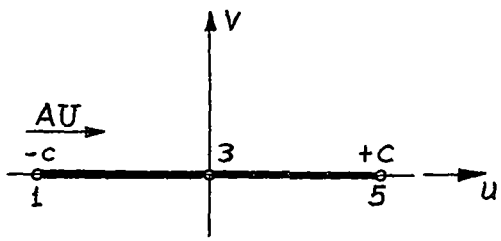

Mapped Plane

The mapping function is

$$x + iy = A\sqrt{u^2 - v^2 + 2iuv - c^2} \quad (i = \sqrt{-1})$$

which maps the points (0-, 0), onto (-C, 0), and (0_+, 0) onto (C, 0). Pt. 3 in the physical plane is mapped onto Pt. 3 of the mapped plane, so

$$0 + ib = A\sqrt{0 - 0 + 0 - C^2} = iAc$$

Therefore $A = \frac{W}{C}$

So the mapping function is

$$x + iy = AF(u,v) = \frac{W}{C}\sqrt{u^2 - v^2 + 2iuv - c^2}$$

Liu has worked out the necessary functions for an inclined baffle, shown in the sketch below

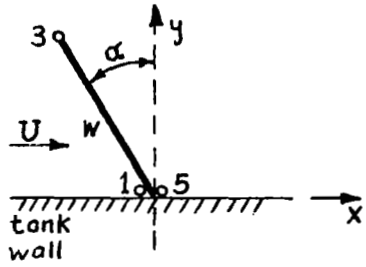

Physical Plane

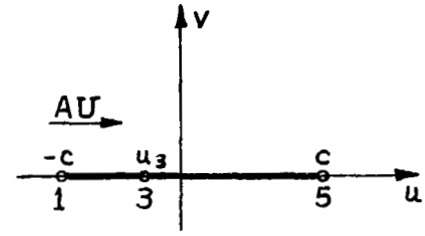

Mapped Plane

The baffle angle $\alpha = \frac{\pi}{n}$

For this case, the necessary functions are

$$K(u,o) = \frac{\sqrt{2}}{2} A (c+u)^{-\frac{n+1}{n}} (c-u)^{-\frac{n-1}{n}}$$

$$R(u,o) = \frac{\sqrt{2}}{2A} \left[\frac{c+u}{c-u}\right]^{\frac{1}{n}} (u-u_3)^{-2}$$

$$f(u,o) = \sqrt{2(c^2-u^2)} \sin\frac{\pi}{n}$$

These functions can be made to apply to the vertical baffle by letting

$n \to \infty$ (i.e., $\alpha \to o$).

So, for the vertical baffle

$$K(u,o) = \frac{\sqrt{2}\,w}{2c} (c^2-u^2)^{-1}$$

$$R(u,o) = \frac{\sqrt{2c}}{2w} u^{-2} \qquad (u_3 = 0 \quad \text{for a vertical baffle})$$

$$f(u,o) = 0$$

Consequently, the baffle pressure is

$$\frac{1}{\rho} p(u,o) = \dot{U} \left\{ Re\left[\frac{w}{c}\sqrt{u^2-c^2}\right] - \frac{w}{c} u \right\} - U^2 \left\{ \frac{3}{2} - \frac{c^2-u^2}{u^2} \right\}$$

But the real part of $\frac{w}{c}\sqrt{u^2-c^2}$ for $|u|<|c|$ is zero.

$$\therefore \frac{1}{\rho} p(u,o) = -\frac{b}{c}\dot{U}_u - U^2\left(\frac{3}{2} - \frac{c^2-u^2}{u^2}\right)$$

The net baffle pressure is the difference between the pressure on the bottom and the pressure on the top, or

$$\frac{1}{\rho} P_{baffle} = P(u+o) - P(u_-,o)$$

$$\frac{1}{\rho} P_{baffle} = -2\frac{w}{c}\dot{U}_u$$

In order to transform this formula back into the physical plane it is necessary to use the mapping function

$$x+iy = \frac{w}{c}\sqrt{u^2-v^2+2iuv-c^2}$$

The baffle is described by $x=0$, $0 \leq y \leq w$, or $v=0, -c \leq u \leq c$

Therefore, on the baffle

$$0+iy = \frac{w}{c}\sqrt{u^2-c^2}$$ or

$$-y^2 = \left(\frac{w}{c}\right)^2(u^2-c^2)$$

$$u = c\sqrt{1-\left(\frac{y}{b}\right)^2}$$ or

So

$$P_{baffle} = -2\rho\,\dot{U} w\sqrt{1-\left(\frac{y}{w}\right)^2}$$

But $U = U_{max}\cos\omega t\cos\theta$

$$\therefore \dot{U} = -\omega U_{max}\sin\omega t\cos\theta$$

$$P_{baffle} = 2\omega\rho U_{max} w\sqrt{1-(y/w)^2} \sin\omega t \cos\theta$$

In terms of the slosh height ζ, $U_{max} = \omega\zeta\rho^{-3.68\frac{d_s}{d}}$

where d_s = depth of baffle below free surface, and d = tank diameter.

Therefore

$$P_{baffle} = 2\omega^2\rho\zeta\rho^{-3.68\frac{d_s}{d}}\sqrt{1-(y/w)^2} \sin\omega t \cos\theta$$

$$= P_{max}\sqrt{1-(y/w)^2} \sin\omega t \cos\theta$$

where $P_{max} = 2\omega^2\rho\zeta\rho^{-3.68\frac{d_s}{d}}$

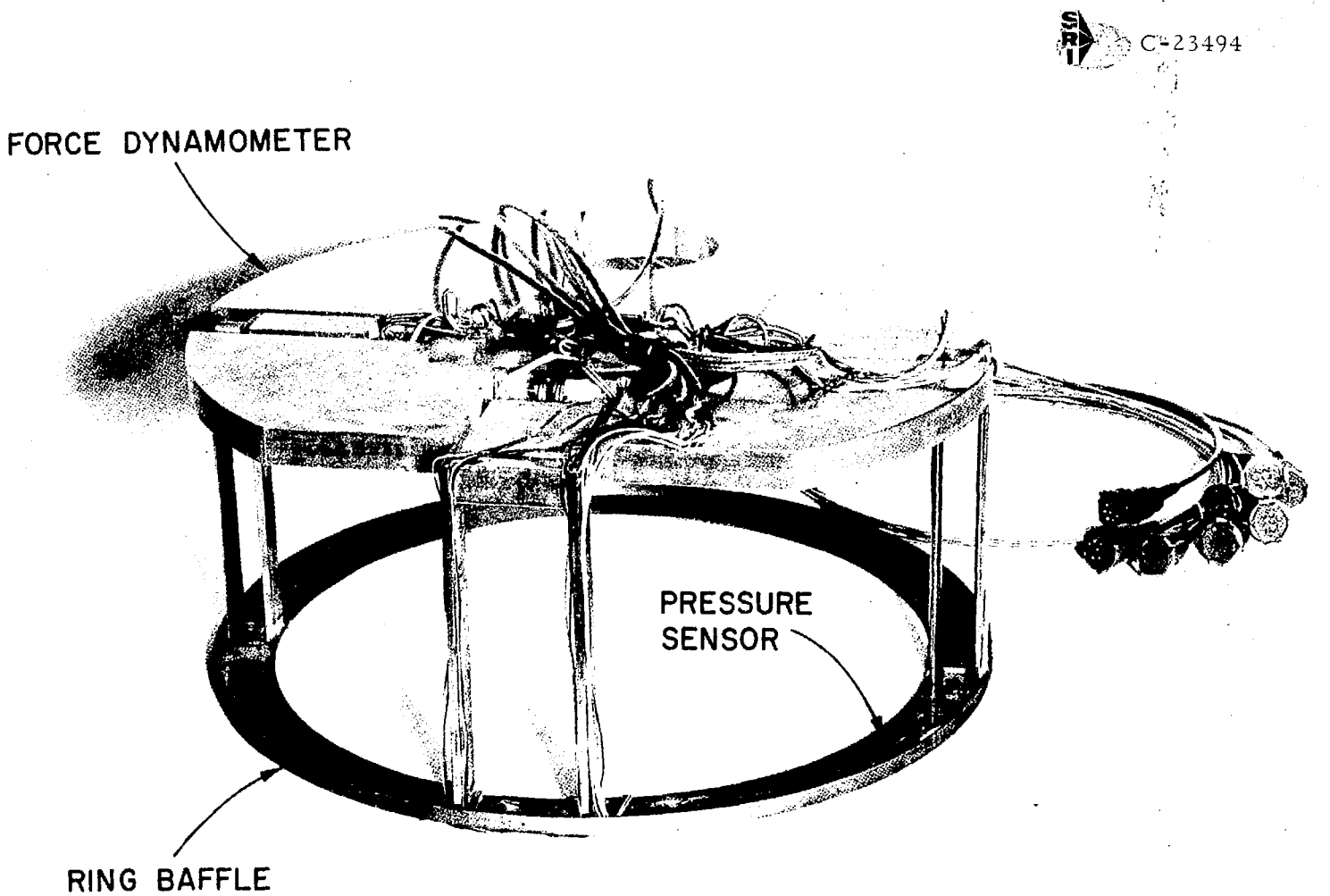

FIGURE 1. RING BAFFLE WITH PRESSURE SENSOR AND HALF-BAFFLE FORCE MEASURING DYNAMOMETER FIXTURE

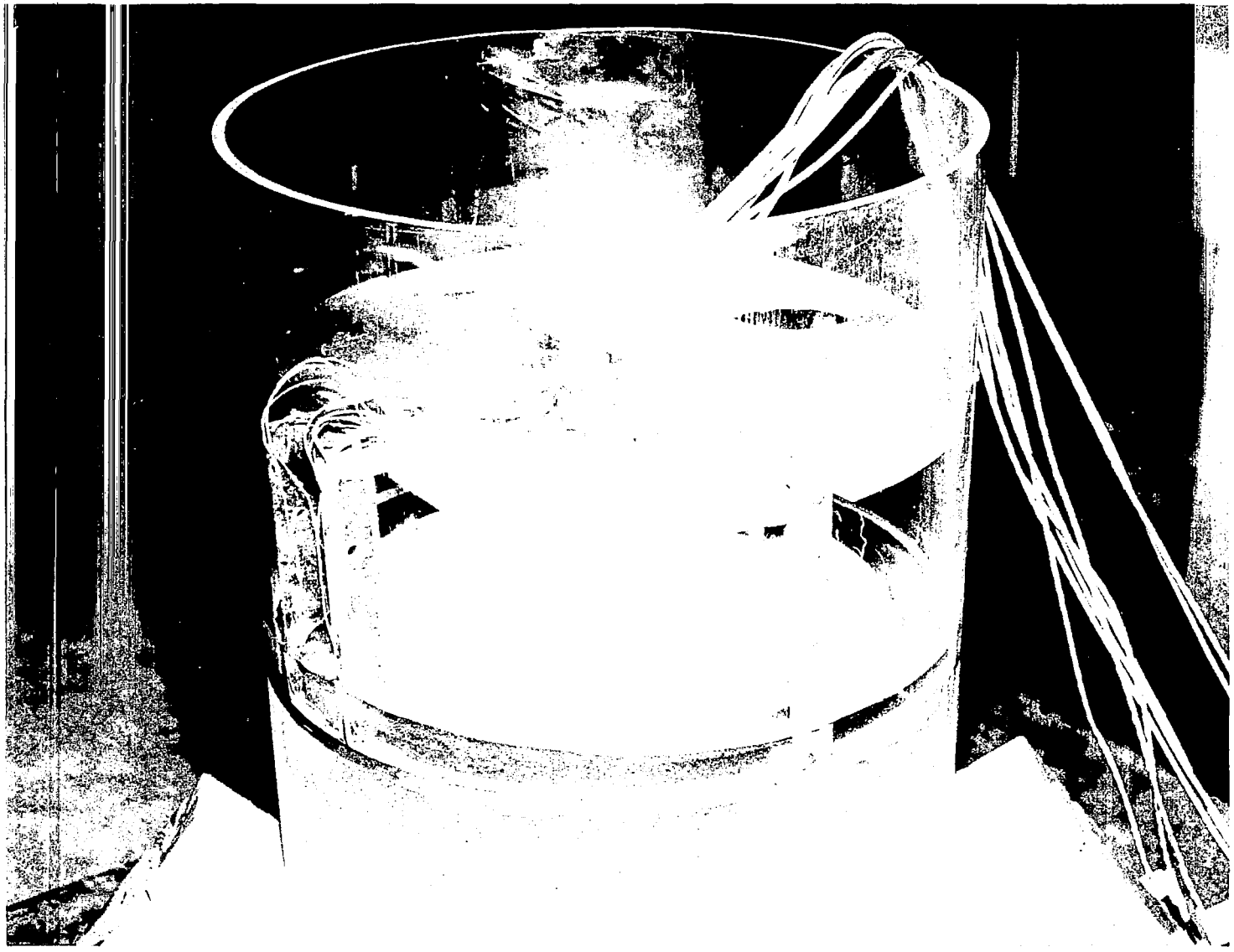

FIGURE 2. ORIENTATION OF BAFFLE PRESSURE AND FORCE DYNAMOMETER FIXTURE UNDER SLOSHING CONDITIONS

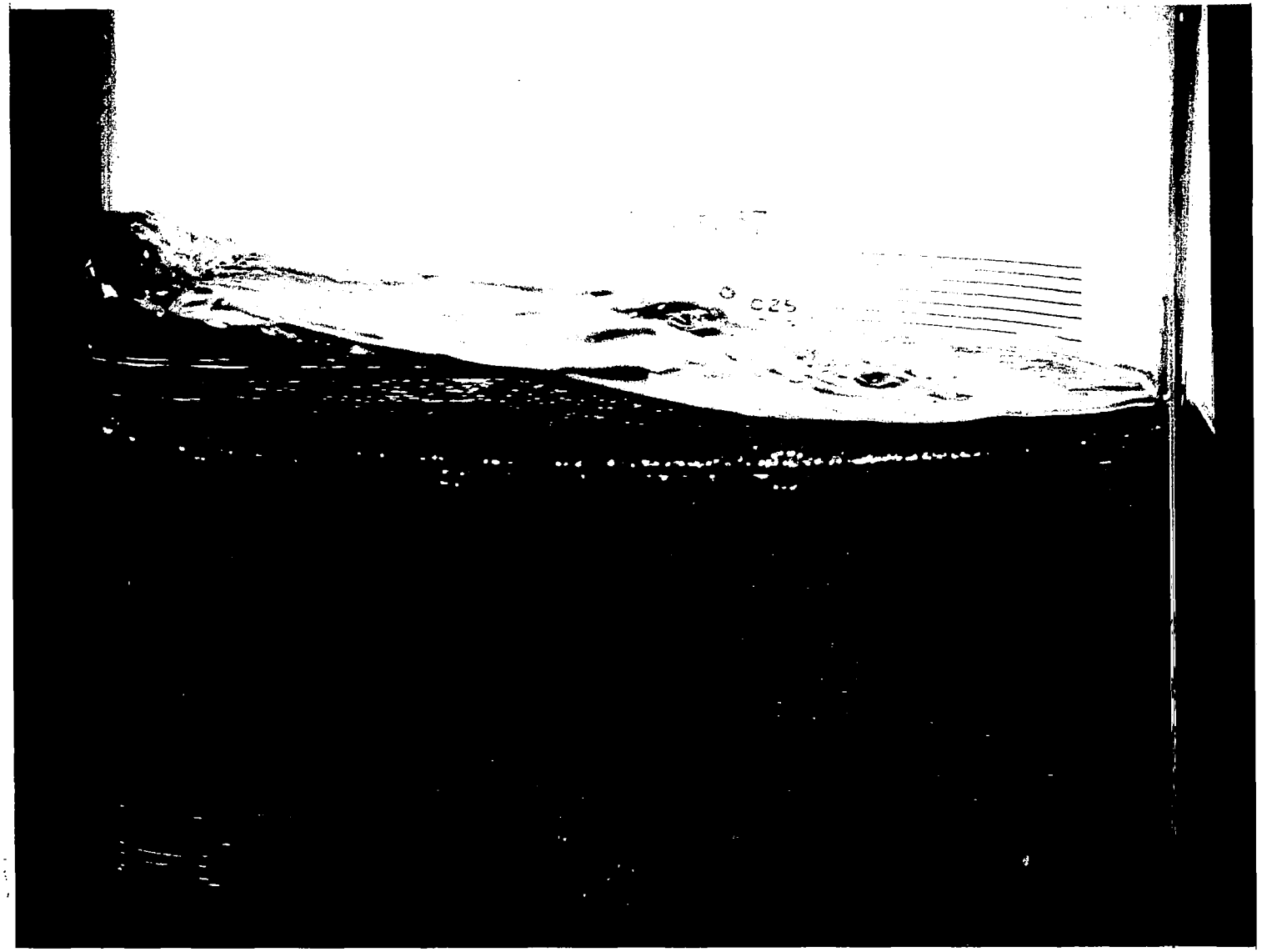

FIGURE 3. COMPLEX SLOSH MODE RESULTING FROM RING BAFFLE SLOSH SUPPRESSION

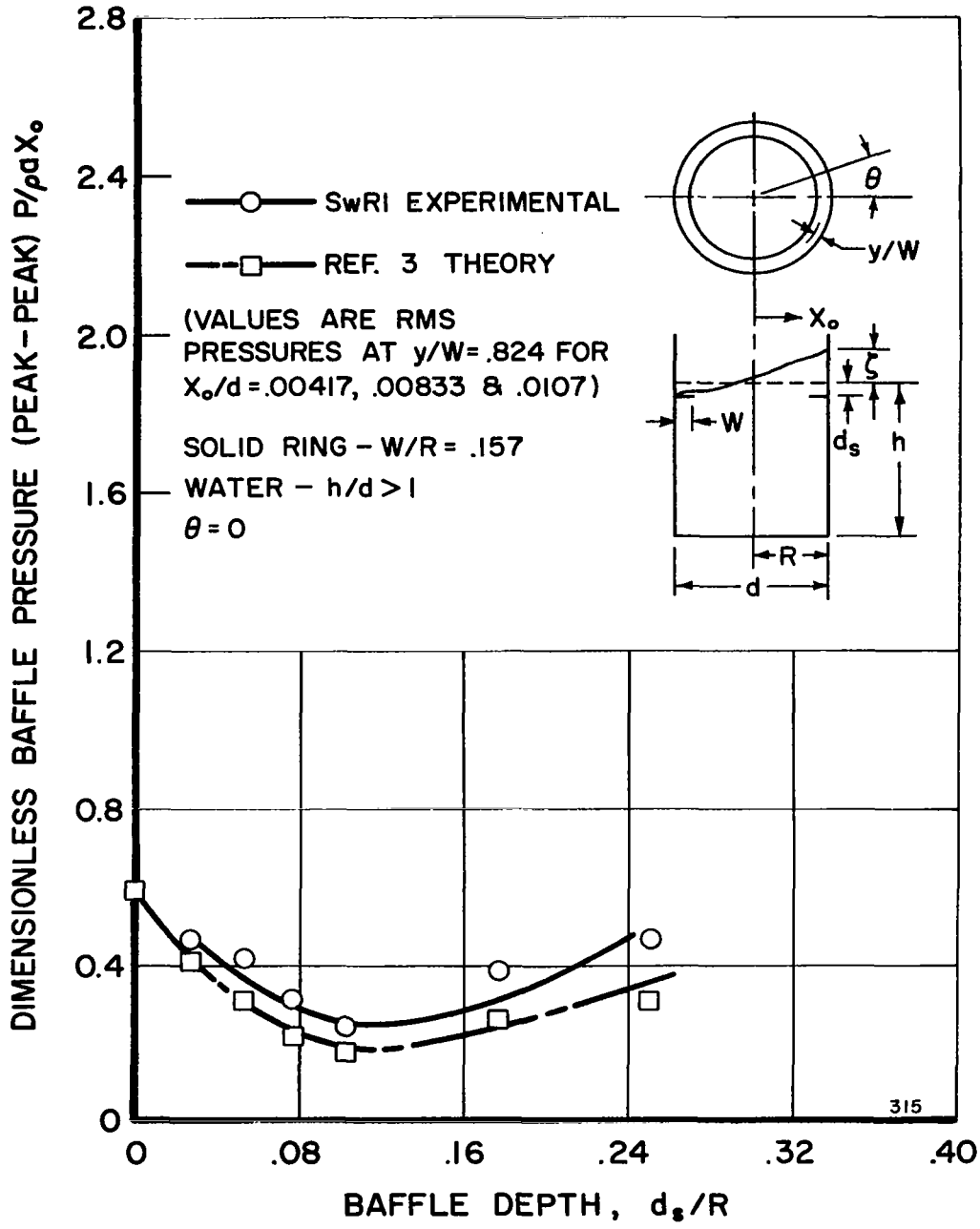

FIGURE 4. COMPARISON OF THEORETICAL AND EXPERIMENTAL BAFFLE PRESSURE FOR y/w = 0.824 AND θ=0° AS A FUNCTION OF BAFFLE DEPTH

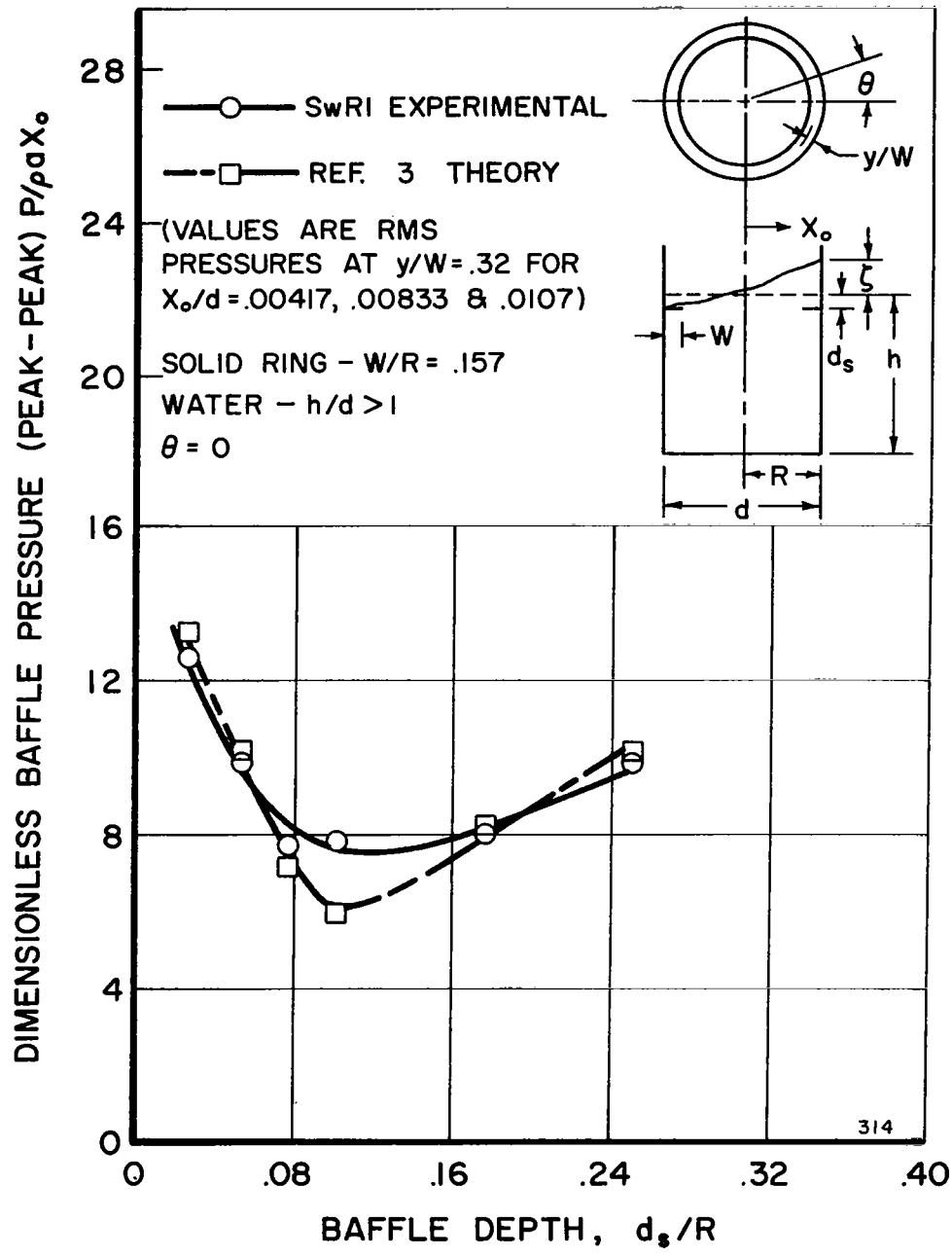

FIGURE 5. COMPARISON OF THEORETICAL AND EXPERIMENTAL BAFFLE PRESSURE FOR y/w = 0.32 AND θ=0° AS A FUNCTION OF BAFFLE DEPTH

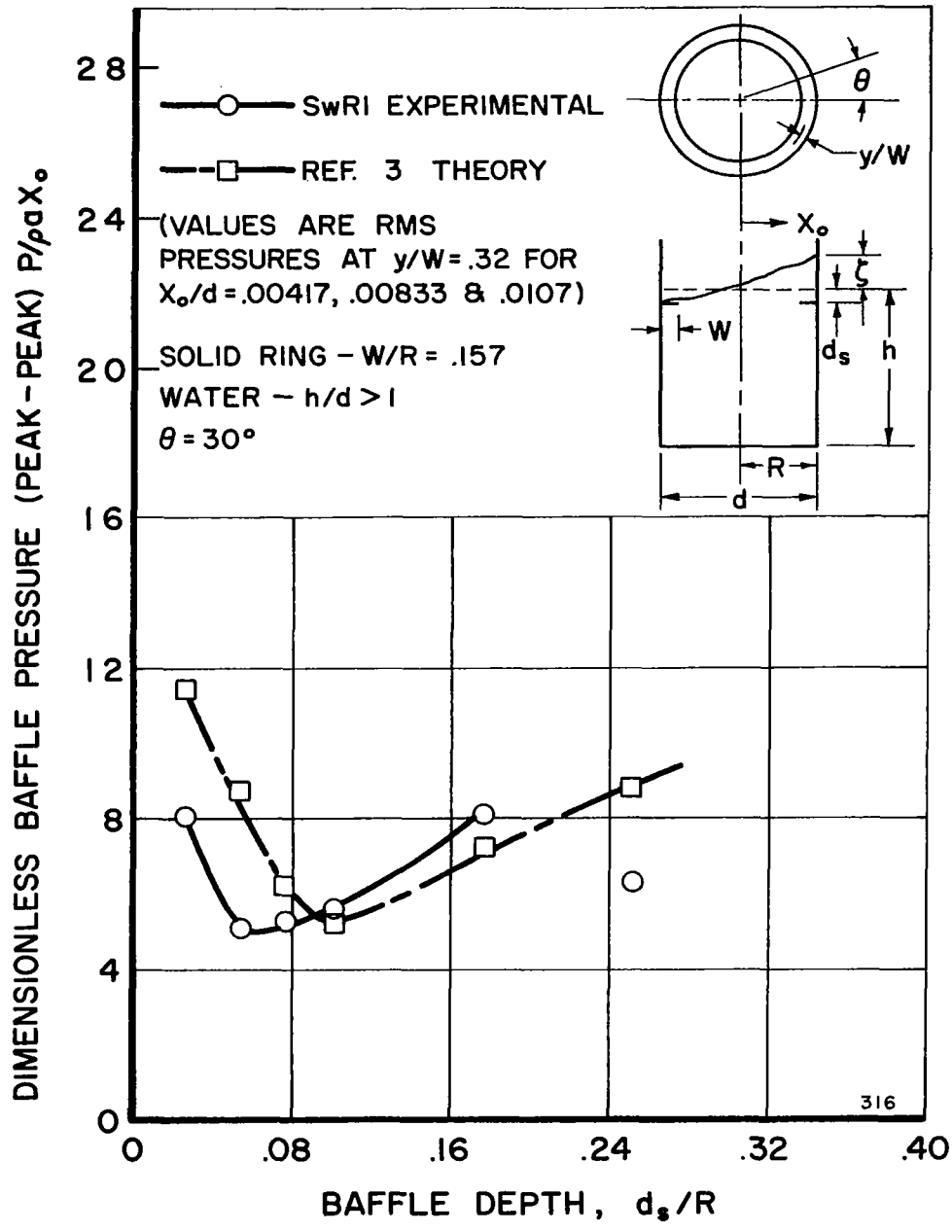

FIGURE 6. COMPARISON OF THEORETICAL AND EXPERIMENTAL BAFFLE PRESSURE FOR y/w = 0.32 AND θ=30° AS A FUNCTION OF BAFFLE DEPTH

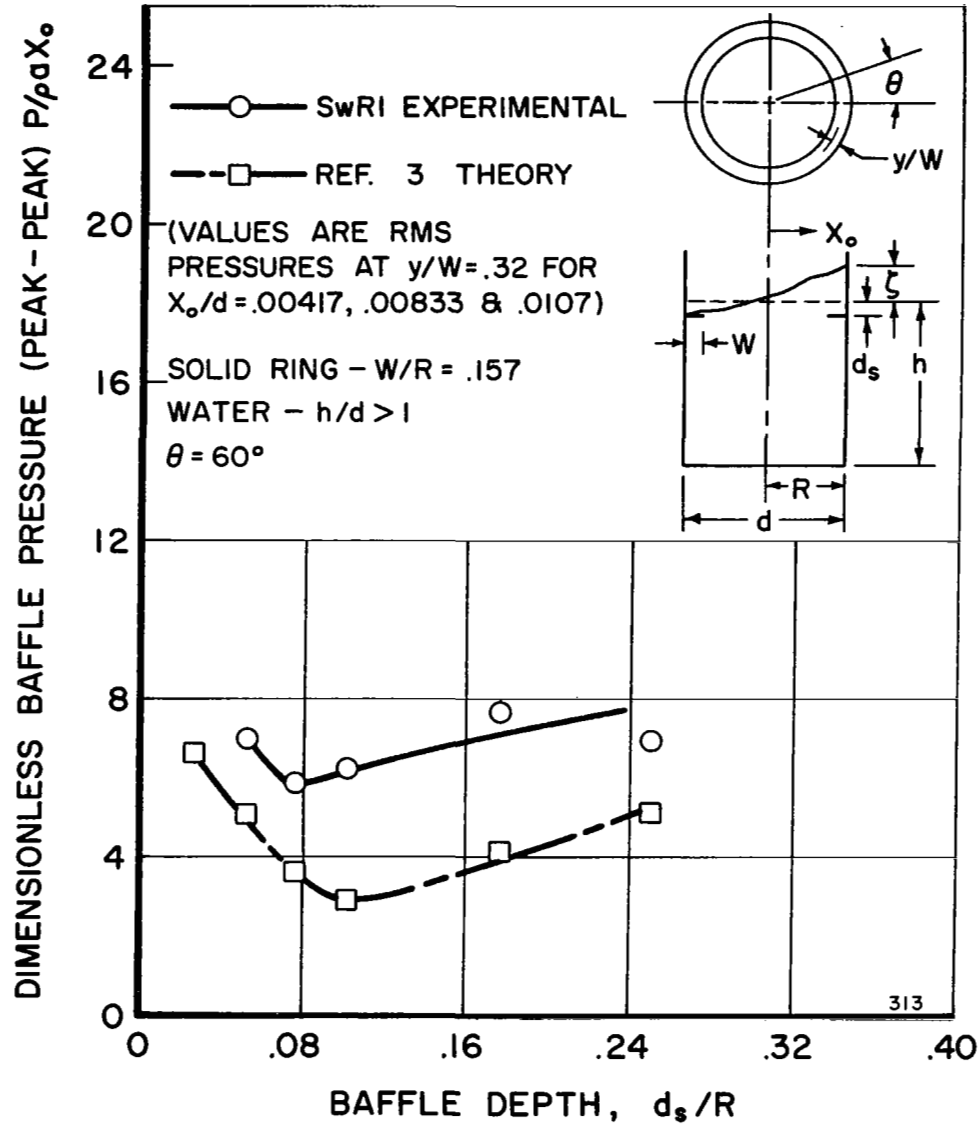

FIGURE 7. COMPARISON OF THEORETICAL AND EXPERIMENTAL BAFFLE PRESSURE FOR y/w = 0.32 AND θ=60° AS A FUNCTION OF BAFFLE DEPTH

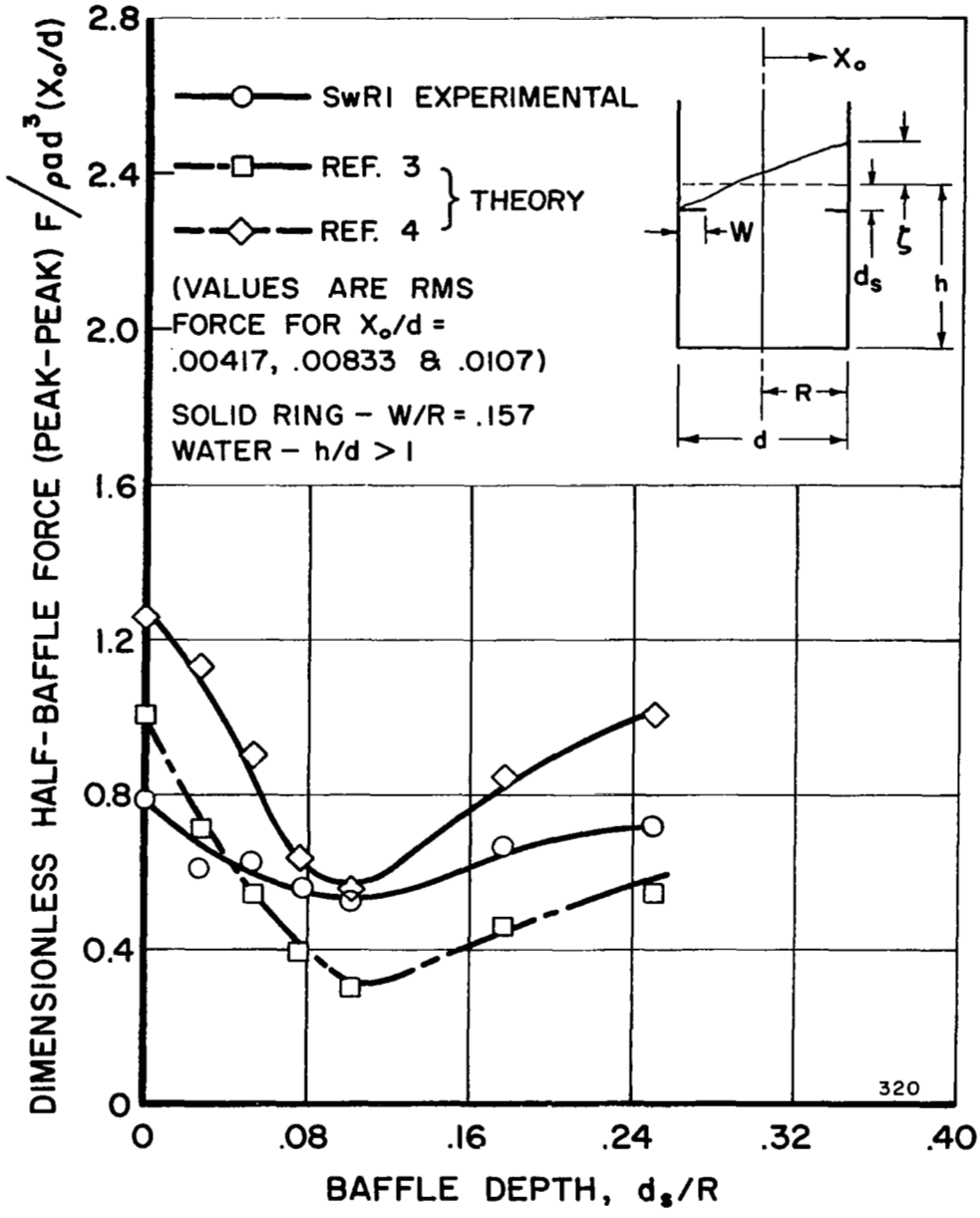

FIGURE 8. COMPARISON OF THEORETICAL AND EXPERIMENTAL HALF-BAFFLE FORCE AS A FUNCTION OF BAFFLE DEPTH

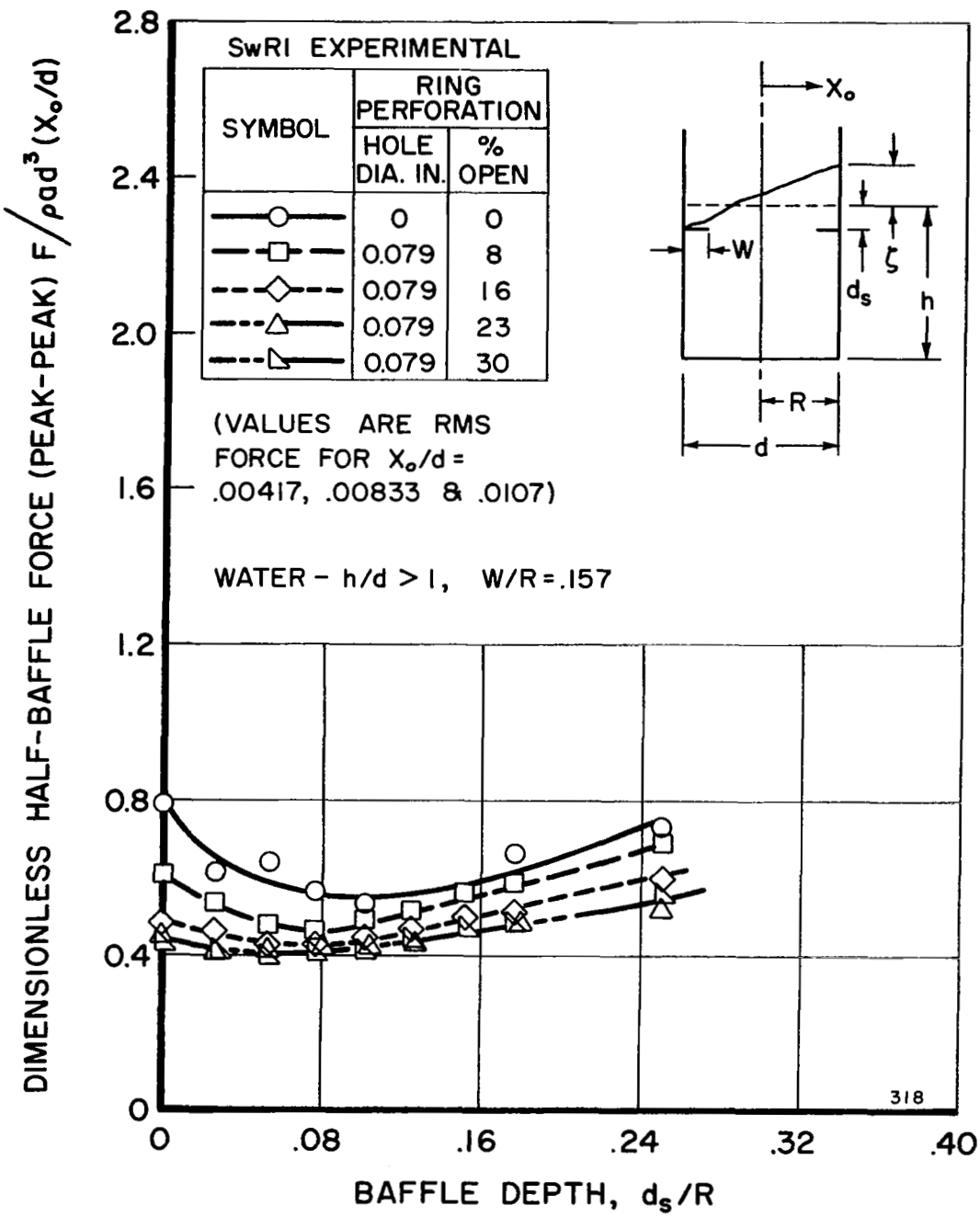

FIGURE 9. EFFECT OF % PERFORATION ON HALF-BAFFLE FORCE AS A FUNCTION OF BAFFLE DEPTH

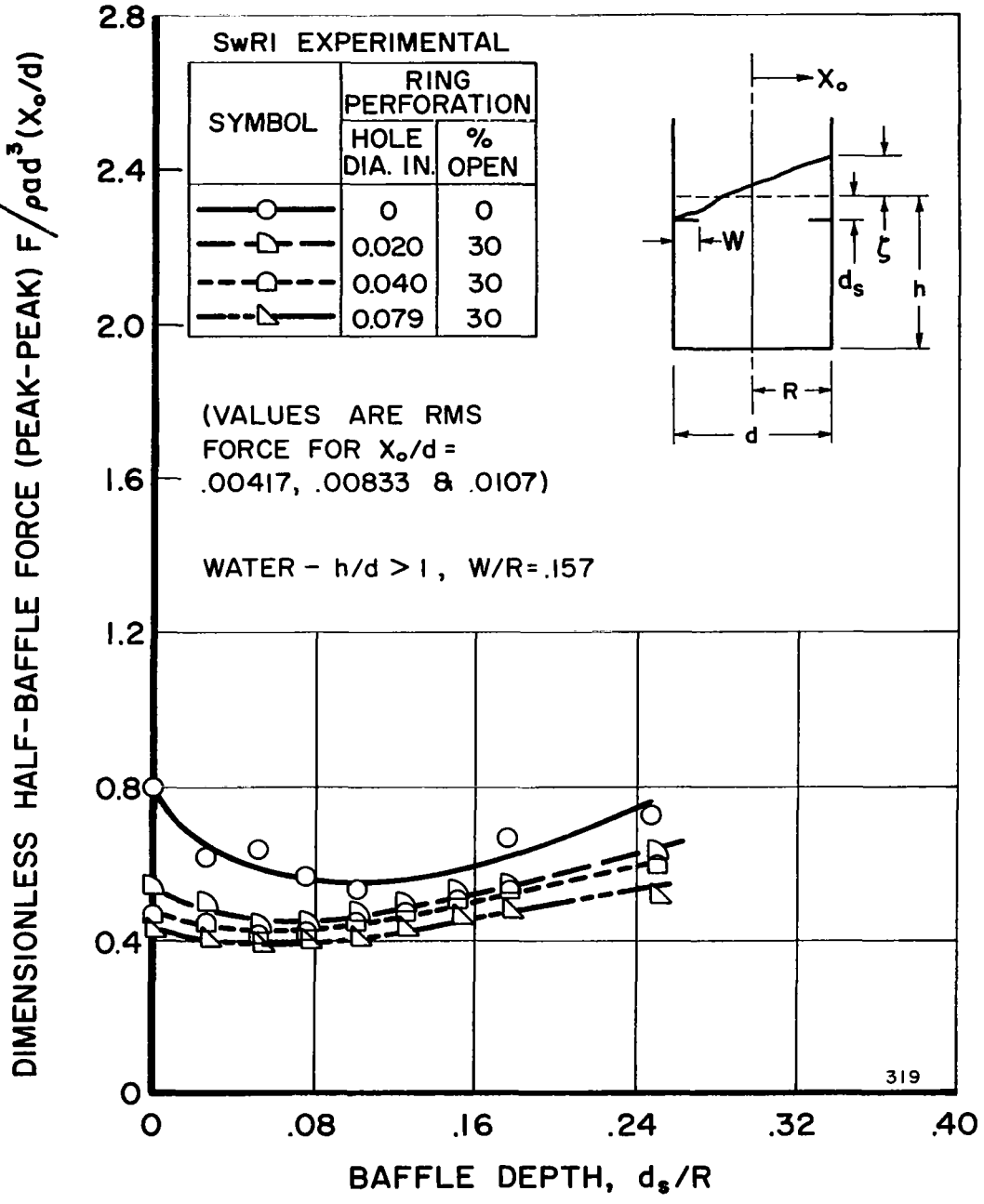

FIGURE 10. EFFECT OF HOLE SIZE ON HALF-BAFFLE FORCE AS A FUNCTION OF BAFFLE DEPTH